Dyes and Pigments 136 (2017) 732–741

Contents lists available at ScienceDirect

Dyes and Pigments

journal homepage: www.elsevier.com/locate/dyepig

Electronic effect on the photophysical properties of 2-(2-hydroxyphenyl)benzothiazole-based excited state intramolecular proton transfer fluorophores synthesized by sonogashira-coupling reaction

Longfei Xu, Qin Wang, Yanrong Zhang*

College of Science, Northwest A&F University, Yangling, Shaanxi 712100, PR China

ARTICLE INFO

Article history:
Received 6 July 2016
Received in revised form
27 August 2016
Accepted 12 September 2016
Available online 15 September 2016

Keywords:
Hammett substituent constant
Solvent effects
Theoretical calculation
Excited state intramolecular proton transfer
Crystal analysis
Sonogashira crossing-coupling reaction

ABSTRACT

For excited-state intramolecular proton transfer (ESIPT) fluorophores, the intramolecular hydrogen bond strength has decisive influence on their photophysical properties. Herein, a series of 2-(2-hydroxyphenyl) benzothiazole (HBT) derivatives as new ESIPT fluorophores are synthesized through Sonogashira-coupling reaction, and their electronic structures are systematically tuned through various substitutions with different Hammett substituent constants (σ) in the 5-position of the phenol ring. Theoretical calculations and crystal analysis show that the HBT derivative with larger σ contains the stronger intramolecular hydrogen bond, which is less likely to be damaged by external factors, and that it has larger energy gap between the highest occupied molecular orbital and the lowest unoccupied molecular orbital. The experimentally observed trends are well in line with the theoretical calculations. More importantly, unlike other HBT derivatives and parent HBT displaying anion emission in PBS medium, the two HBT derivatives bearing methyl ester and cyano substitutions, respectively, emit as keto tautomer, which are expected to be applied in biological aspects.

1. Introduction

Excited-state intramolecular proton transfer (ESIPT) fluorophores have attracted significant attention in fundamental investigation and have been applied in luminescence materials [1,2], fluorescent probes [3–6], laser dyes [7,8] and UV filtering [9,10], etc. Compared with the ordinary fluorophores, ESIPT fluorophores are usually very sensitive to the surrounding medium and show large Stokes shifts (>150 nm) because of their unique four-lever photophysical process [11,12]. ESIPT is a photo-induced tautomerization. In the excited state, the enol tautomer bearing an intramolecular H-bond between the hydroxyl proton and the electronegative atom, is converted to the keto tautomer through the migration of the hydroxyl proton to the electronegative atom in the subpico second time scale [13,14]. Then the keto tautomer in the excited state is relaxed to its ground state, followed by the recovery to the energetically favored enol tautomer via ground state intramolecular proton transfer (GSIPT) to complete the four-level process [15]. Therefore, in the ESIPT molecules, the intramolecular H-bond donors and acceptors in close proximity are vital to the ESIPT process [8,16], and the intramolecular H-bond strength has decisive influence on their photophysical properties.

2-(2-hydroxyphenyl)benzimidazole (HBI) [17–19], 2-(2-hydroxyphenyl) benzoxazole (HBO) [20–22] and 2-(2-hydroxyphenyl)benzothiazole (HBT) [23,24] are well-known ESIPT fluorophores. Their photophysical properties have been studied extensively to elucidate the ESIPT mechanism [25–28]. Recently, their chemical modification has been of particular interest to study ESIPT toward biochemical application. Park et al. synthesized two HBO derivatives through Knoevenagel condensation of aldehyde-substituted HBO with cyano-acetic acid 2-ethyl-hexyl ester and malononitrile, respectively, and they observed that the keto emission showed large bathochromic shift with increasing solvent polarity [29]. Zhao et al. reported a HBT derivative with boron-dipyrromethene substituent, which shows no ESIPT effect [30]. Later, Zhao et al. prepared another HBT derivative with naphthalimide substituent, which shows red-shifted absorption/emission in comparison with parent HBT, but its emission is completed quenched in protic solvent methanol, due to the significant intramolecular charge transfer character (ICT) [31]. Wang

* Corresponding author.
E-mail address: zhangyr@nwsuaf.edu.cn (Y. Zhang).

http://dx.doi.org/10.1016/j.dyepig.2016.09.024
0143-7208/

et al. modified the 4- and 5-position of HBT with three substituted amino group including dimethylamino, diphenylamino and carbazole group, respectively, and studied the effect of the different electron-donating amino groups on their photophysical properties [32]. However, they merely studied their property in solid and the synthetic strategy cannot be conveniently exploited to introduce other substituted groups. Based on the previous reports and the ESIPT mechanism, it is obvious that the subtle structural change of the HBT derivatives may cause dramatic effect on their fluorescence properties [33]. However, to date, very few studies have been performed on the systematic modulating of the fluorescence properties of HBT derivatives. In this regard, it is still in great demand to design a series of structurally diverse HBT derivatives through a facile and efficient strategy to investigate electronic effect on their photophysical properties.

Considering the general features of copper-palladium catalyzed Sonogashira coupling reaction of terminal alkynes with aryl halides [34–38]: the exceptional functional group compatibility and the introduction of extended π-conjugation, we employ this synthetic protocol to achieve two goals simultaneously. Various substituents with different Hammett substituent constants (σ) can be conveniently introduced into the HBT framework; and the introduction of the C≡C linker would ensure efficient electronic communication between the HBT moiety and aryl moiety [31].

Herein, eight HBT derivatives with different σ are obtained, and their molecular structures are shown in Scheme 1. Their photophysical properties are studied in detail in various solvents. All of these derivatives exhibit typical ESIPT property, and the derivative with larger σ shows blue-shifted fluorescence spectra with improved fluorescence quantum yield, and the increasing relative intensity ratio of keto emission and enol emission. To reveal the electronic effect on their photophysical properties, theoretical calculations and crystal analysis are also conducted, which demonstrate that the derivative with larger σ contains a stronger intramolecular H-bond and a larger HOMO-LUMO energy gap.

2. Experimental

2.1. Materials

Methyl 4-iodobenzoate and trimethylsilylacetylene were purchased from Heowns (Tianjin, China). 2-aminothiophenol, salicylaldehyde, 5-bromosalicylaldehyde, $PdCl_2(PPh_3)_2$, CuI, *N,N*-dimethylaniline, 4-Iodoanisole, 4-Iodotoluene, Iodobenzene, 1-chloro-4-iodobenzene, 4-Iodobenzotrifluoride and 4-Iodobenzonitrile were purchased from Energy Chemical (Shanghai, China). All other materials were purchased from local commercial suppliers and were of analytical reagent grade, unless otherwise stated. Solvents were purified by standard procedures. Ultrapurified water was supplied by a Milli-Q system (Millipore). All reactions were monitored by thin-layer chromatography (TLC) with detection by UV or by iodine.

2.2. Instruments

^1H and ^{13}C NMR spectra of the products were recorded on a Bruker 500 MHz NMR spectrometer in $CDCl_3$ solution using tetramethylsilane (TMS) as the internal standard, and chemical shifts were given in ppm and coupling constants (*J*) in Hz. High resolution Mass spectra (HRMS) were recorded on a Bruker instrument using standard conditions (electron spray ionization, ESI). UV absorption spectra were obtained on a UV–vis spectrophotometer (U-3310). The fluorescence spectra were recorded on a fluorospectrophotometer (F-7000). The fluorescence quantum yield (Φ_f) in solution was determined by using quinine sulfate ($\Phi_f = 0.55$ in 0.1 M H_2SO_4) as a standard [39].

2.3. Theoretical calculation

The ground state (S_0) and the first singlet excited state (S_1) geometries of the enol and keto tautomers of HBT and its derivatives were optimized in the gas phase using density functional theory (DFT) and time-dependent density functional theory (TDDFT) at the B3LYP/6-31 + G(d) level, respectively.

2.4. Single crystal X-ray diffraction

The single crystals of compounds HBT-H and HBT-Me were obtained by the slow diffusion of their respective CH_2Cl_2/hexane solution for several days at room temperature. The data collection was done at room temperature on a Bruker SMART APEX-II CCD area detector using graphite-monochromated Mo Kα radiation (λ = 0.71073 Å). Data reduction and integration were done by the INTEGRATE program of the $APEX_2$ software. Semi-empirical absorption correction was applied using the SCALE program. The structure was solved by direct method and refined by the full matrix least-squares method on F_2 using SHELX.

2.5. Synthesis and characterization

2.5.1. 2-(2-hydroxyphenyl)benzothiazole (HBT)

It was synthesized according to previously reported method [40]. ^1H NMR (500 MHz, $CDCl_3$): δ 12.506 (s, 1H), 8.044 (d, *J* = 8.0 Hz, 1H), 7.955 (d, *J* = 8.0 Hz, 1H), 7.752 (dd, *J* = 7.5, 1.5 Hz, 1H), 7.577–7.543 (m, 1H), 7.480–7.418 (m, 2H), 7.160 (dd, *J* = 8.5, 1.0 Hz,

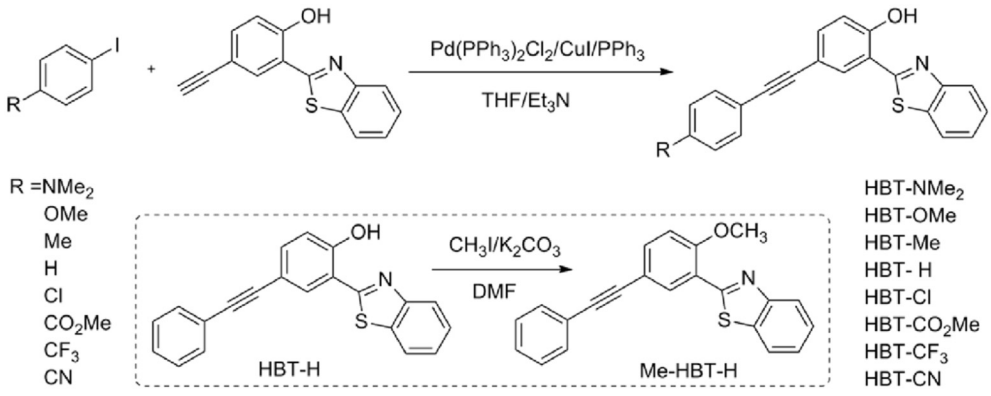

Scheme 1. Synthetic routes and molecular structures of the HBT derivatives and Me-HBT-H.

1H), 7.027–6.994 (m, 1H).

2.5.2. 2-(5-ethnyl-2-hydroxyphenyl) benzothiazole

It was synthesized in a three-step reaction from the starting material 5-bromosalicylaldehyde according to previously reported methods [40,41]. ^{1}H NMR (500 MHz, $CDCl_3$): δ 12.854 (s, 1H), 8.053 (d, J = 8.0 Hz, 1H), 7.979 (d, J = 8.0 Hz, 1H), 8.053 (d, J = 8.0 Hz, 1H), 7.908 (d, J = 2.0 Hz, 1H), 7.595–7.562 (m, 1H), 7.548 (dd, J = 8.5, 2.0 Hz, 1H), 7.507–7.475 (m, 1H), 7.112 (d, J = 8.5 Hz, 1H), 3.112 (s, 1H).

2.5.3. N,N-dimethyl-4-iodo aniline

It was synthesized according to previously reported method [34]. ^{1}H NMR (500 MHz, $CDCl_3$): δ 7.513 (d, J = 8.5 Hz, 2H), 6.538 (d, J = 8.5 Hz, 2H), 2.967 (s, 6H).

2.5.4. General procedure for the preparation of the HBT derivatives

Under nitrogen atmosphere, $Pd(PPh_3)_2Cl_2$ (17.6 mg, 0.025 mmol, 5.0 mol %), PPh_3 (13.1 mg, 0.05 mmol, 10.0 mol%), CuI (9.6 mg, 0.005 mmol, 10.0 mol %), TEA (5 mL) and substituted iodobenzene (0.6 mmol) were added to a solution of 2-(5-ethnyl-2-hydroxyphenyl) benzothiazole (125.5 mg, 0.5 mmol) in anhydrous THF (10 mL). The mixture was stirred at 70 °C overnight and cooled to rt. The solvent was removed under reduced pressure and the residue was purified by column chromatography to give the terminal product.

2.5.4.1. 4-((3-(benzo[d]thiazol-2-yl)-4-hydroxyphenyl)ethynyl)benzonitrile (HBT-CN). Pale yellow, crystalline solid. Yield: 65.3% (114 mg). HRMS (ESI) m/z calcd for $C_{22}H_{13}N_2OS$ $(M + H)^+$ 353.07431, found 353.07431.^{1}H NMR (500 MHz, $CDCl_3$): δ 12.935 (s, 1H), 8.060 (d, J = 8.5 Hz, 1H), 7.985 (d, J = 8.0 Hz, 1H), 7.705–7.657 (m, 4H), 7.602–7.571 (m, 2H), 7.499 (t, J = 7.5 Hz, 1H), 7.161 (d, J = 8.5 Hz, 1H). ^{13}C NMR (125 MHz, $CDCl_3$) 168.3, 158.8, 151.6, 136.0, 132.6, 132.1, 131.97, 131.92, 128.3, 127.0, 126.0, 122.4, 121.7, 118.6, 118.5, 117.1, 113.4, 111.4, 93.1, 87.1.

2.5.4.2. 2-(benzo[d]thiazol-2-yl)-4-((4-(trifluoromethyl)phenyl)ethynyl)phenol (HBT-CF_3). Pale yellow, crystalline solid. Yield: 70.2% (138 mg). HRMS (ESI) m/z calcd for $C_{22}H_{13}F_3NOS$ $(M + H)^+$ 396.06645, found 396.06616.^{1}H NMR (500 MHz, $CDCl_3$): δ 12.884 (s, 1H), 8.068 (d, J = 8.0 Hz, 1H), 7.989 (d, J = 7.5 Hz, 1H), 7.951 (d, J = 1.5 Hz, 1H), 7.708–7.660 (m, 4H), 7.614–7.586 (m, 2H), 7.514–7.482 (m, 1H), 7.161 (d, J = 8.5 Hz, 1H). ^{13}C NMR (125 MHz, $CDCl_3$) 168.4, 158.6, 151.7, 135.9, 132.7, 131.8, 131.7, 127.2, 126.9, 125.9, 125.4, 125.3, 125.1, 122.4, 121.6, 118.5, 117.0, 113.8, 91.0, 87.2.

2.5.4.3. Methyl 4-((3-(benzo[d]thiazol-2-yl)-4-hydroxyphenyl) ethynyl)benzoate (HBT-CO_2Me). Pale yellow, crystalline solid. Yield: 57.6% (110 mg). HRMS (ESI) m/z calcd for $C_{23}H_{16}NO_3S$ $(M + H)^+$ 386.08454, found 386.08453.1H NMR (500 MHz, $CDCl_3$): δ 12.880 (s, 1H), 8.087 (d, J = 8.0 Hz, 2H), 8.065 (d, J = 9.0 Hz, 1H), 7.992 (d, J = 8.0 Hz, 1H), 7.953 (d, J = 2.0 Hz, 1H), 7.657 (d, J = 8.5 Hz, 2H), 7.615–7.570 (m, 2H), 7.514–7.484 (m, 1H), 7.159 (d, J = 8.5 Hz, 1H), 3.986 (s, 3H). 13C NMR (125 MHz, CDCl3) 168.4, 166.6, 158.5, 151.7, 136.0, 132.7, 131.8, 131.4, 129.6, 129.5, 128.0, 126.9, 125.9, 122.4, 121.7, 118.4, 117.0, 113.9, 91.6, 87.9, 52.2.

2.5.4.4. 2-(benzo[d]thiazol-2-yl)-4-((4-chlorophenyl)ethynyl)phenol (HBT-Cl). Pale yellow, crystalline solid. Yield: 61.8% (111 mg). HRMS (ESI) m/z calcd for $C_{21}H_{13}ClNOS$ $(M + H)^+$ 362.04009, found 362.04001.^{1}H NMR (500 MHz, $CDCl_3$): δ 12.857 (s, 1H), 8.056 (d, J = 8.0 Hz, 1H), 7.982 (d, J = 8.0 Hz, 1H), 7.922 (d, J = 1.5 Hz, 1H), 7.596–7.580 (m, 2H), 7.526 (d, J = 8.5 Hz, 2H), 7.507–7.474 (m, 1H), 7.388 (d, J = 8.0 Hz, 2H), 7.144 (d, J = 8.5 Hz, 1H). ^{13}C NMR (125 MHz, $CDCl_3$) 168.5, 158.3, 151.7, 135.8, 134.3, 132.7, 132.7, 131.6, 128.8, 126.9, 125.9, 122.3, 121.8, 121.7, 118.4, 117.0, 114.2, 89.5, 87.4.

2.5.4.5. 2-(benzo[d]thiazol-2-yl)-4-(phenylethynyl)phenol (HBT-H). Pale yellow, crystalline solid. Yield: 74.8% (122 mg). HRMS (ESI) m/z calcd for $C_{21}H_{14}NOS$ $(M + H)^+$ 328.07906, found 328.07901.^{1}H NMR (500 MHz, $CDCl_3$): δ 12.840 (s, 1H), 8.058 (d, J = 8.0 Hz, 1H), 7.985 (d, J = 8.0 Hz, 1H), 7.941 (d, J = 2.0 Hz, 1H), 7.617–7.563 (m, 4H), 7.507–7.476 (m, 1H), 7.438–7.378 (m, 3H), 7.146 (d, J = 8.5 Hz, 1H). ^{13}C NMR (125 MHz, $CDCl_3$) 168.5, 158.0, 151.6, 135.8, 132.6, 131.5, 131.5, 128.4, 128.2, 126.8, 125.8, 123.2, 122.3, 121.6, 118.2, 116.9, 114.5, 88.4.

2.5.4.6. 2-(benzo[d]thiazol-2-yl)-4-(p-tolylethynyl)phenol (HBT-Me). Pale yellow, crystalline solid. Yield: 70.5% (120 mg). HRMS (ESI) m/z calcd for $C_{22}H_{16}NOS$ $(M + H)^+$ 342.09471, found 342.09473.^{1}H NMR (500 MHz, $CDCl_3$): δ 12.802 (s, 1H), 8.055 (d, J = 8.0 Hz, 1H), 7.982 (d, J = 8.0 Hz, 1H), 7.929 (d, J = 1.5 Hz, 1H), 7.593–7.560 (m, 2H), 7.506–7.470 (m, 3H), 7.223 (d, J = 8.0 Hz, 2H), 7.135 (d, J = 8.5 Hz, 1H), 2.430 (s, 3H). ^{13}C NMR (125 MHz, $CDCl_3$) 168.6, 158.0, 151.7, 138.4, 135.9, 132.7, 131.5, 131.5, 129.2, 126.9, 125.8, 122.3, 121.7, 120.2, 118.3, 116.9, 114.7, 88.7, 87.8, 21.6.

2.5.4.7. 2-(benzo[d]thiazol-2-yl)-4-((4-methoxyphenyl)ethynyl) phenol (HBT-OMe). Pale yellow, crystalline solid. Yield: 67.8% (121 mg). HRMS (ESI) m/z calcd for $C_{22}H_{16}NO_2S$ $(M + H)^+$ 358.08963, found 358.08957.^{1}H NMR (500 MHz, $CDCl_3$): δ 12.796 (s, 1H), 8.057 (d, J = 8.0 Hz, 1H), 7.985 (d, J = 7.5 Hz, 1H), 7.921 (d, J = 2.0 Hz, 1H), 7.595–7.564 (m, 2H), 7.551–7.434 (m, 2H), 7.505–7.472 (m, 1H), 7.133 (d, J = 9.0 Hz, 1H), 6.947 (d, J = 9.0 Hz, 2H), 3.891 (s, 3H). ^{13}C NMR (125 MHz, $CDCl_3$) 168.4, 159.5, 157.7, 135.7, 132.9, 132.6, 131.3, 126.8, 126.754, 125.73, 125.70, 122.2, 121.6, 121.5, 118.2, 116.8, 1140, 88.1, 87.0, 55.3.

2.5.4.8. 2-(benzo[d]thiazol-2-yl)-4-((4-(dimethylamino)phenyl)ethynyl)phenol (HBT-NMe_2). Brown, crystalline solid. Yield: 51.4% (95 mg). HRMS (ESI) m/z calcd for $C_{23}H_{19}N_2OS$ $(M + H)^+$ 371.12126, found 371.12097.^{1}H NMR (500 MHz, $CDCl_3$): δ 12.746 (s, 1H), 8.051 (d, J = 8.0 Hz, 1H), 7.980 (d, J = 8.0 Hz, 1H), 7.908 (d, J = 2.0 Hz, 1H), 7.564 (dd, J = 8.5, 1.5 Hz, 2H), 7.495–7.469 (m, 3H), 7.118 (d, J = 8.5 Hz, 1H), 6.728 (d, J = 9.0 Hz, 2H), 3.052 (s, 6H). ^{13}C NMR (125 MHz, $CDCl_3$) 168.9, 157.5, 151.8, 150.2, 150.1, 146.4, 135.7, 132.7, 131.2, 126.8, 125.7, 122.3, 121.6, 118.2, 116.8, 111.9, 89.6, 86.3, 40.3.

2.5.5. Synthesis and characterization of 2-(2-methoxy-5-(phenylethynyl)phenyl)benzo[d]thiazole (Me-HBT-H)

The mixture of HBT-H (68 mg, 0.20 mmol), K_2CO_3 (55 mg, 0.4 mmol) and *N,N*-dimethyl formamide (2 mL) were stirred at room temperature, then iodomethane (31 μL, 0.50 mmol) was added. The mixture were stirred at 40 °C for 20 min, then the resulting solution was poured into ice water. The mixture was extracted with CH_2Cl_2 three times. The organic layer was washed with saturated NaCl aqueous solution and then dried over anhydrous Na_2SO_4. The solvent was removed under reduced pressure then the crude product was purified by column chromatography (silica gel, petroleum: CH_2Cl_2, 4: 1, v/v) to give the product as white solid. Yield: 96% (65 mg). ^{1}H NMR (500 MHz, $CDCl_3$): δ 8.796 (d, J = 2.0 Hz, 1H), 8.164 (d, J = 8.0 Hz, 1H), 7.986 (d, J = 7.5 Hz, 1H), 7.767 (dd, J = 8.5, 2.5 Hz 1H), 7.600 (dd, J = 8.0, 1.5 Hz 2H), 7.573–7.541 (m, 1H), 7.455–7.424 (m, 4H), 7.095 (d, J = 8.5 Hz, 1H) 4.131 (s, 3H),. ^{13}C NMR (125 MHz, $CDCl_3$) δ 162.2, 157.0, 152.1, 136.2, 134.8, 132.9, 131.58, 128.4, 128.2, 126.1, 124.9, 123.4, 122.9, 122.5, 121.3, 116.4, 111.8, 88.9, 88.7, 55.9.

3. Results and discussion

3.1. Synthesis and characterization of the HBT derivatives

These HBT derivatives were synthesized using Sonogashira-coupling reaction between para-substituted iodobenzenes and 2-

(5-ethnyl-2-hydroxyphenyl)benzothiazole [41]. The control compound Me-HBT-H was prepared by methylation of HBT-H in the presence of CH_3I and K_2CO_3. The synthetic procedures are shown in Scheme 1 and characterizations (^1H NMR, ^{13}C NMR, HRMS) are summarized in Supporting Information (SI, Figs. S13–S38). X-ray single-crystal analysis was also performed for HBT-Me and HBT-H, others can not grow into a suitable single crystal.

3.2. Comparison of photophysical properties of HBT-H and HBT

To study the electronic effect of substituents with different σ in the 5-position of the phenol ring of HBT on the photophysical property, we first recorded the absorption and emission spectra of HBT-H in several solvents (PhMe, $CHCl_3$, CH_2Cl_2, ACN, MeOH) possessing different polarities and H-bonding abilities, and characterized the effect of solvation on the steady-state spectroscopic property. As shown in Fig. 1a, the absorption spectra of HBT-H almost have similar profiles in these solvents studied here except for MeOH. There are two main absorption peaks, and the low energy absorption band is due to the S_0–S_1 (π-π*) transition of the intramolecular H-bonding closed enol tautomer (E-E*, Scheme 2). The absorption of HBT-H (353–358 nm) is red-shifted compared with that of HBT (332–336 nm) (Fig. 1c), which is due to the extended π-conjugation by the introduction of phenyl alkynyl group [37,38]. In MeOH, a lower energy absorption band appears for HBT-H, which can be assigned to the deprotonated anion species (A-A*, Scheme 2) due to the solvent-assisted deprotonation interaction [42,43]. However, the absorption peak of anion species is not observed in MeOH solution of HBT, which might be due to its weaker acidity in comparison with HBT-H. It should be noted that the phenolic hydroxyl proton of HBT-H (12.840 ppm) lies in the lower field compared with that of HBT (12.560 ppm) in ^1H NMR spectra (Fig. S22 and Fig. S10). To further verify the assignment of the anion species, the absorption spectrum is recorded in more polar solvent DMF that has high basicity (large β value, 0.74) [44], and the more intensive peak around 438 nm appeares. The similar phenomenon is also observed in other HBT derivatives [7,45].

The emission spectra of HBT-H are depending on the solvent properties to a large extent (Fig. 1b). The yellow emission with large Strokes shifts of ca. 185 nm is predominant in nonpolar PhMe, and in medium polarity solvent $CHCl_3$ and CH_2Cl_2, which is typical characteristic of ESIPT emission from keto tautomer (K*-K, Scheme 2), and the emission is red-shifted about 30 nm compared with the green emission (513–515 nm) of HBT (Fig. 1d). As shown in Scheme 2, the K* state derived from E* state via the ESIPT process, is relaxed to K state through keto emission, followed by GSIPT to the more stable E state. The keto and enol emission bands are both detected in ACN. While in protic polar MeOH, HBT-H gives another kind of dual emission, where besides the shorter enol emission around

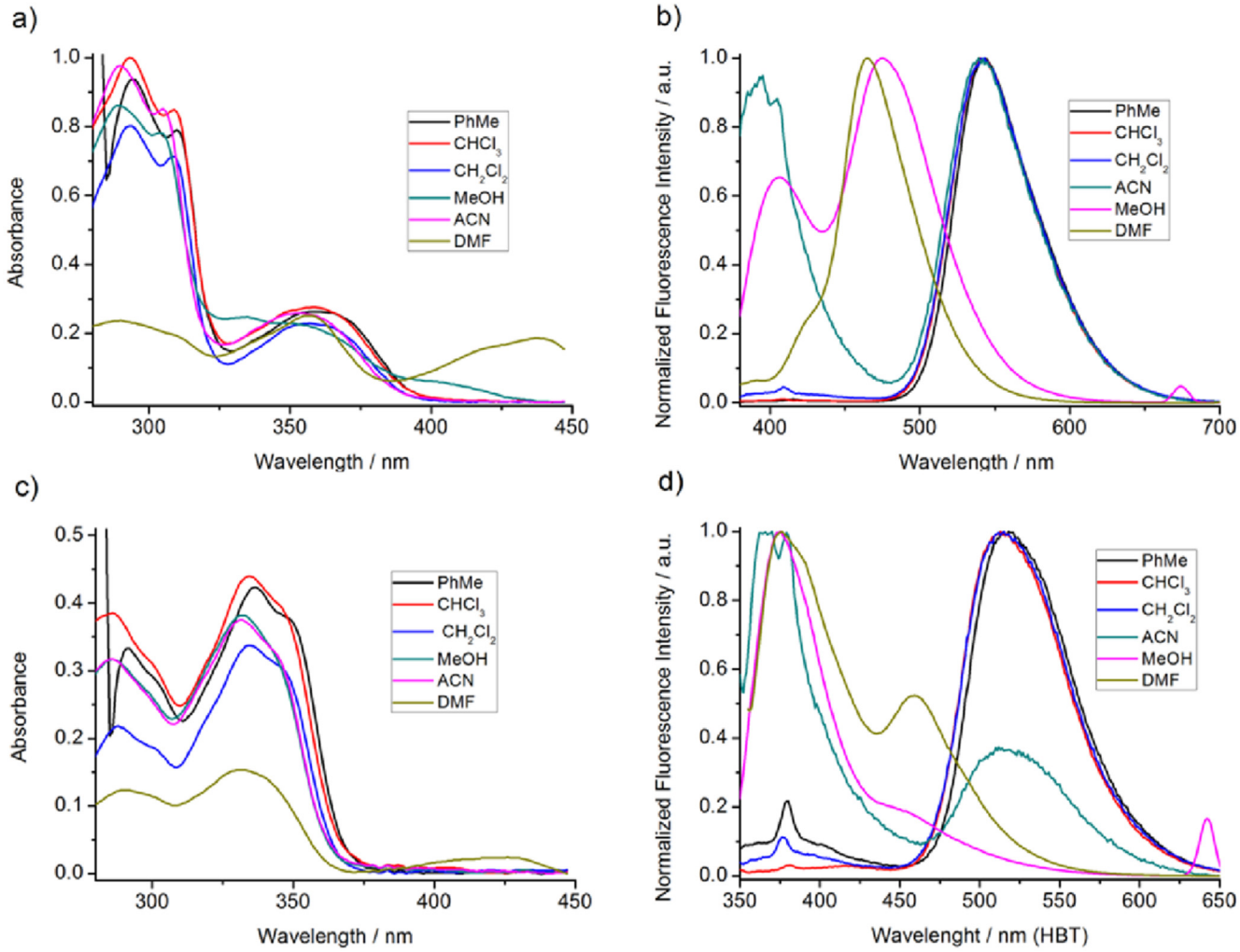

Fig. 1. Absorption (a/c) and fluorescence (b/d) spectra of HBT-H (top) and HBT (bottom) in various solvents.

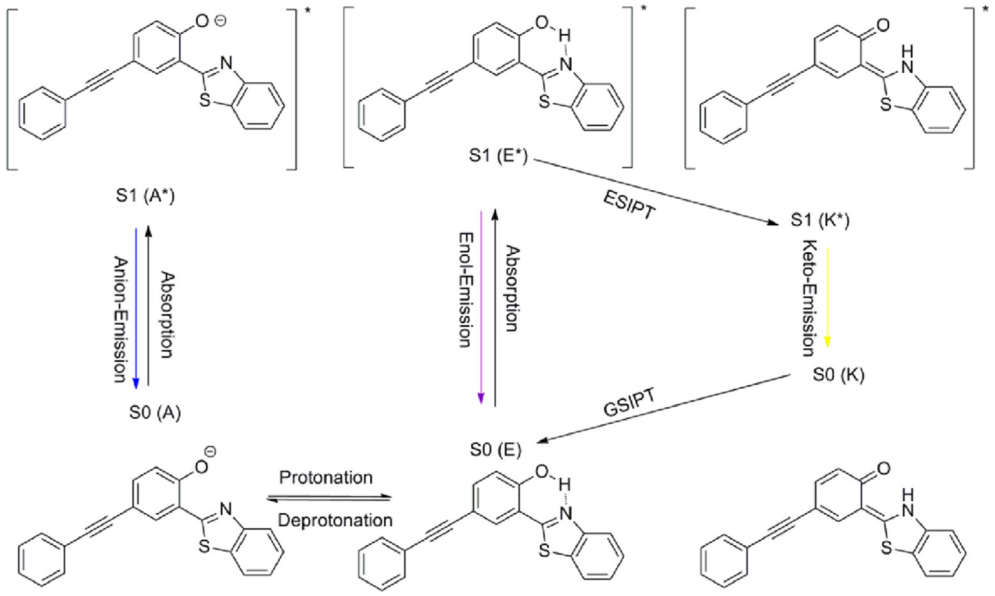

Scheme 2. Schematic representation of the photophysical process for HBT-H.

407 nm, the keto emission is not observed and a new emission peak at 475 nm assigned to the emission of the anion species (A*-A, Scheme 2) appeares. To verify this assignment, the emission spectrum of HBT-H was also recorded in more polar DMF. When it was excited at 357 nm, the strong emission band at 465 nm was observed. Just as reported in previous literatures, that the proton is transferred from the oxygen atom to the N atom of the intramolecular H-bonding closed enol tautomer is necessary for the transformation from enol tautomer to keto tautomer at excited state [46]. In non-H-bonding solvents, such as PhMe, $CHCl_3$, CH_2Cl_2, which are unable to effectively compete for the phenolic hydroxyl proton with the N atom of the benzothiazole (BT) ring, excitation results in very efficient keto emission. However, in ACN, which can act as the H-bond acceptor, the phenolic hydroxyl of HBT-H may form an intermolecular H-bond with the solvent molecule, therefore emission from enol and keto tautomers are both detected. The excitation spectra of HBT-H recorded in different solvents (Fig. S1) resemble their respective corresponding absorption spectra, revealing that the three kinds of fluorescence emission all originate from the ground state absorbing species. Additionally, the control compound Me-HBT-H shows almost solvent-independent absorption and blue-shifted emission with normal Strokes shift (~30 nm) due to the methoxy group (Fig. S2), which is in agreement with the lack of ESITP and indicates that the phenolic hydroxyl is crucial in HBT-H for its solvent-dependent fluorescent property.

3.3. The electronic effect of substituents on the photophysical properties

To gain an understanding of the correlation of the substituent electronic effects with the photophysical properties of ESIPT fluorophores, the electronic structures of the HBT derivatives are systematically tuned through various substituents with different σ in the 5-position of the phenol ring (Scheme 1). In this study, the selected substituents are CN, CF_3, CO_2Me, Cl, H, Me, OMe and NMe_2 with respective σ of 0.66, 0.54, 0.45, 0.23, 0.0, -0.17, -0.27 and −0.83 in turn [47]. It is noted that with the σ value increasing, the acidity of the HBT derivative should increase accordingly, which is verified by the chemical shift of the phenolic hydrogen proton (Table 1 and Figs. S10–S34) and consistent with the results of theoretical calculation (vida infra). Therefore, it can be concluded that the strength of the intramolecular H-bond is redoubled in the HBT derivative with large σ [48]. The photophysical data of the new series of HBT derivatives are summarized in Table 1.

In non-H-bonding solvents, such as PhMe, $CHCl_3$ and CH_2Cl_2, the keto emission is predominant (Fig. 2a–2c). The HBT derivative with smaller σ shows red-shifted fluorescence spectra and has decreased fluorescence quantum yield (Φ_f), and the HBT derivative with larger σ shows the opposite trend (Table 1). For example in PhMe, the λ_{max} of HBT-NMe_2 with −0.83 σ is 568 nm and its Φ_f is 0.19%, while the λ_{max} of HBT-CN with 0.66 σ blue-shifts to 538 nm and its Φ_f increases

Table 1
Experimental photophysical data of the new series of HBT derivatives.

Substituent group	NMe_2	OMe	Me	H	Cl	CO_2Me	CF_3	CN
σ	−0.83	−0.27	−0.17	0.00	0.23	0.45	0.54	0.66
Chemical shift	12.746	12.796	12.802	12.840	12.857	12.880	12.884	12.935
λ_{ex} in PhMe	568	549	546	543	542	539	538	538
Φ_f in PhMe (%)	0.19	0.52	1.08	1.28	1.83	2.52	2.70	2.89
λ_{ex} in $CHCl_3$	571	551	546	542	541	538	536	536
λ_{ex} in CH_2Cl_2	578	550	546	543	541	539	537	537
λ_{ex} in ACN	568/417	549/412	545/396	539/395	540/391	537/389	537/390	535/389
I_K/I_E in ACN	0.628	0.802	0.827	1.053	1.167	1.219	1.313	1.321
λ_{ex} in MeOH	404/498/-	422/468/-	410/471/-	407/475/-	405/474/-	398/462/529	402/469/-	396/460/528
I_A/I_E in MeOH	9.216	0.883	0.956	1.531	2.075	–	2.391	–
λ_{ex} in PBS/ACN	497	480	475	479	476	546	470	540

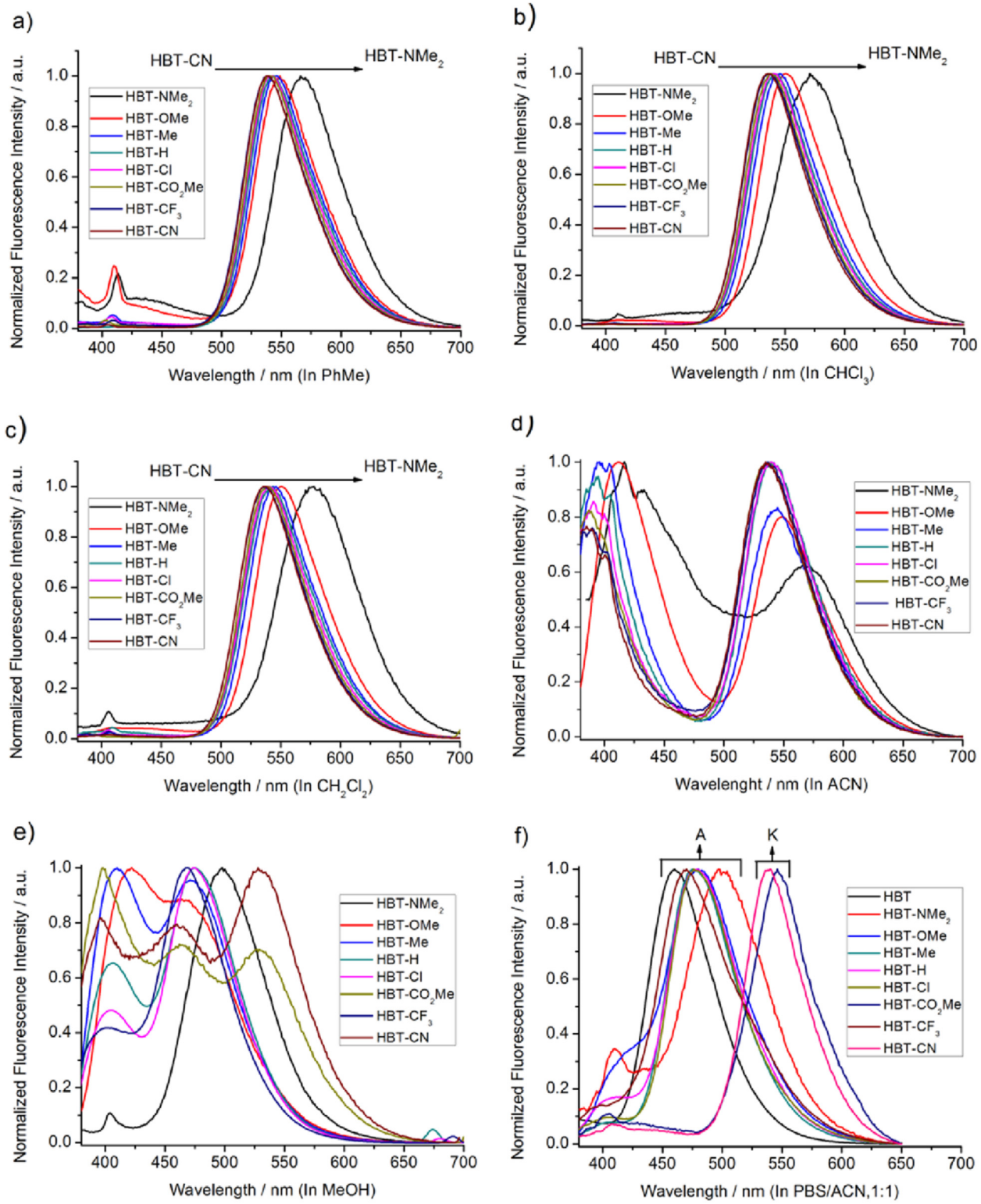

Fig. 2. Comparison of fluorescence emission of the new series of HBT derivatives in various solvents: a) PhMe, b) $CHCl_3$, c) CH_2Cl_2, d) ACN, e) MeOH and f) PBS/ACN (v/v, 1/1). Excitation at the respective maximum absorption wavelength of the enol tautomer (see Fig. S3).

to 2.89%. These results further demonstrate that the HBT derivative with larger σ should contain the stronger intramolecular H-bond. Because the previous reports point out that, in ESIPT fluorophores, the H-bond strength is often proportional to Φ_f; the stronger the H-bonds are, the higher the Φ_f values [49,50].

In ACN, which can act as H-bond acceptor, the fluorescence spectra of all the HBT derivatives consist of two emission bands at 389–417 nm (enol emission) and 535–568 nm (keto emission), and the relative intensity ratio of keto emission and enol emission (I_K/I_E) is electronic effect dependent (Fig. 2d). And the ratio is increased

for the HBT derivative with large σ (Table 1). For example, the ratio is 0.628 for HBT-NMe_2 and increases to 1.321 for HBT-CN. We envisaged that the reinforced strength of intramolecular H-bond in the HBT derivative with larger σ, is less likely to be destroyed by solvent molecules, which provides the prerequisite for ESIPT fluorophores to produce keto emission.

The emission of some HBT derivatives is completely quenched in protic polar solvent MeOH due to the significant intramolecular charge transfer (ICT) [31]. Therefore, we further studies their photophysical property in MeOH. From Fig. 2e, it is obvious that the emission of these HBT derivatives are not at all quenched. For HBT-OMe, HBT-Me, HBT-H, HBT-Cl and HBT-CF_3, they show dual emission, originating from anion species and enol tautomer, respectively, and with the increase of σ value, the fluorescence intensity ratio of anion species and enol tautomer (I_A/I_E) increases accordingly. For example, the ratio is 0.883 for HBT-OMe, while the ratio increases to 2.391 for HBT-CF_3. This result manifests that the substituent with large σ accelerates the deprotonation process to form anion species. While HBT-NMe_2 with the smallest σ shows almost single anion emission, we conjecture the possible reason is that the intermolecular H-bond between the phenolic hydroxyl and the N atom of the NMe_2 group is stronger than the intramolecular H-bond of the phenolic hydroxyl and the N atom in the BT ring, due to the stronger basicity of the NMe_2 group compared with the N atom in the BT ring. While for HBT-CN with the largest σ, three kinds of emission were detected simultaneously, originating from enol tautomer (396 nm), anion species (460 nm) and keto tautomer (528 nm), respectively. HBT-CO_2Me with the σ between that of HBT-Cl and HBT-CF_3, also shows three emission peaks at 398 nm, 462 nm and 529 nm, respectively. Considering the change trends of fluorescent spectra of other HBT derivatives in ACN and MeOH, it could be concluded that the substituent group with large σ, on one hand accelerates the deprotonated progress to form anion species to produce anion emission, on the other hand strengthens the intramolecular H-bond to facilitate ESIPT to produce keto emission. Therefore, the fluorescence difference we observed for HBT-CN, HBT-CF_3 and HBT-CO_2Me might be due to the subtle balance between the deprotonation process of phenolic hydroxyl, intermolecular H-bond with solvent molecule MeOH and intramolecular H-bond with the N atom in the BT ring, which cause the anion emission, enol emission and keto emission, respectively, as shown in Scheme 2.

In order to facilitate the application of these new HBT derivatives in biological aspects, we are keen to study their emission in PBS medium and detect their fluorescence emission in PBS/ACN (v/v, 1/1) (Fig. 2f). These HBT derivatives all show sole emission. HBT-CF_3, HBT-Cl, HBT-H, HBT-Me, HBT-OMe and HBT-NMe_2 display anion emission at 470–497 nm, which is the same as parent HBT [3,51] (Fig. S4), while HBT-CO_2Me and HBT-CN emit as keto emission at 546 nm and 540 nm, respectively. These assignment is also verified by comparison of their respective absorption spectrum and excitation spectrum (Fig. S5). The excitation peaks of HBT-CO_2Me and HBT-CN are from the neutral enol tautomer, while the other excitation peaks are from the anion species. Therefore, HBT-CO_2Me and HBT-CN might be applied in various biological aspects.

3.4. Theoretical calculations for HBT derivatives

To further take insight into the electronic effect on the photophysical properties of HBT derivatives, DFT/TDDFT calculations have been carried out. The ground-state and the lowest singlet excited-state geometries of these HBT derivatives and parent HBT were optimized with DFT and TDDFT methods at the B3LYP/6-31 + G(d) level, respectively. The calculations reproduce the experimentally observed trends.

The optimized S_0 and S_1 state geometry of the enol form of HBT-CN is shown in Fig. 3a as an example and that of other HBT derivatives and HBT are shown in Fig. S6. Both in S_0 state and in S_1 state, the aryl alkynyl moiety and the BT ring are near coplanar with the phenol ring, indicating that aryl alkynyl moiety indeed could extent the π-conjugation of HBT. Therefore, these HBT derivatives possess red-shift absorption/emission compared with parent HBT. Regarding to the structural parameters involved in the intramolecular H-bond (O—H···N), the bond length of O—H and the distance between hydroxy proton and the N atom in the BT ring (H···N) in S_0 and S_1 state, are shown in Fig. 3b and 3c, respectively, and their respective change magnitude from S_0 to S_1 are listed in Table S1. It is noted that the bond length of O—H in S_0 becomes longer in the HBT derivative with larger σ, which is consistent with the change trend of chemical shift of the phenolic hydroxyl proton; and the distance of H···N becomes shorter. For example, in HBT-NMe_2 with −0.83 σ, the bond length of O—H is 0.99375 Å and the distance of H···N is 1.83995 Å; while in HBT-CN with 0.66 σ, the bond length of O—H is 0.99558 Å and the distance of H···N is 1.74347 Å. Therefore, for the HBT derivative with larger σ, which has longer bond length of O—H and shorter distance of H···N, its intramolecular H-bond strength should be more stronger and be less likely to be damaged by external factors, such as solvent molecules [52]. This presents a very good explanation of the increasing relative intensity ratio of keto emission and enol emission for the HBT derivative with large σ in ACN. As mentioned in previous literatures, in ESIPT fluorophores, Φ_f is often proportional to the H-bond strength [50,51]. Therefore, the above-mentioned theoretical results might also provide a reasonable explanation for the difference in Φ_f between the HBT derivatives. When excited from S_0 to S_1, the bond length of O—H is elongated, the distance of N···H becomes shorter, and the change magnitude is more distinguished for the HBT derivative with larger σ. For example, the bond length of O—H in HBT-OMe with −0.27 σ is elongated from 0.99413 Å in S_0 to 1.02674 Å in S_1 with 0.03261 Å of change magnitude, and the distance of N···H is shorten from 1.7507 Å in S_0 to 1.62006 Å in S_1 with 0.13064 Å of change magnitude; while the bond length of O—H in HBT-CN with 0.66 σ constant is elongated from 0.99558 Å in S_0 to 1.04674 Å in S_1 with 0.05116 Å of change magnitude, and the distance of N···H is shorten from 1.74347 Å in S_0 to 1.56016 Å in S_1 with 0.18331 Å of change magnitude. These structural changes indicate that the intramolecular H-bond in the HBT derivative with large σ is substantially strengthened in the S_1 state, resulting in more efficient keto emission. In HBT-NMe_2, from S_0 to S_1 the change magnitude of the distance of N···H is 0.19198 Å, which is larger than that of other HBT derivatives, at present the reason for this deviation is not obvious.

The highest occupied molecular orbital (HOMO) and the lowest unoccupied molecular orbital (LUMO) of the enol tautomers of HBT and HBT derivatives are calculated and that of HBT-CN is depicted in the left side of Fig. 3d as an example, that of other HBT derivatives and HBT are shown Fig. S7. These HBT derivatives have similar electron distribution of molecular orbitals. The HOMO is distributed on the phenol ring and the aryl alkynyl moiety, and is barely present on the BT ring. In contrast, the LUMO is mainly spread over the phenol ring and the BT ring, and is barely present on the aryl alkynyl moiety. Additionally, from HOMO to LUMO, the electron density of the oxygen atom of the phenolic hydroxyl decreases, while the electron density of the N atom in the BT ring increases. These calculated results manifest that the basicity of the N atom in the BT ring and the acidity of the phenolic hydroxyl both improved in S_1, which would facilitate ESIPT from the oxygen atom to the N atom.

The HOMO and LUMO of the keto tautomers of HBT and HBT derivatives are also calculated, and that of HBT-CN is depicted in the

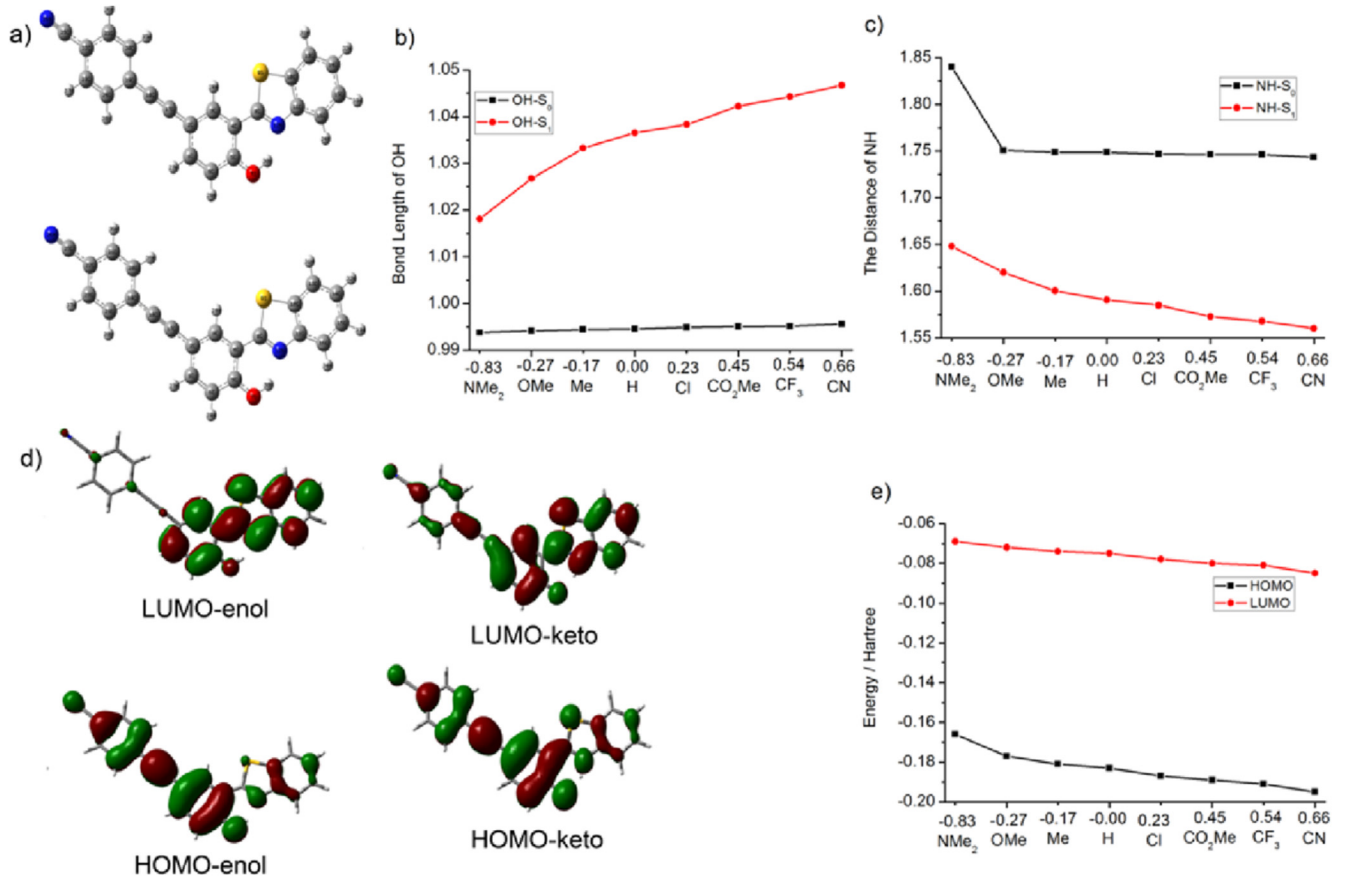

Fig. 3. a) Optimized molecular structure of the enol tautomer of HBT-CN in S_0 (bottom) and S1 (up) states, b) The bond length of OH of the HBT derivatives in S_0 and S_1 by theoretical calculation, c) The distance of NH of the HBT derivatives in S_0 and S_1 by theoretical calculation, d) DFT-calculated HOMO and LUMO of the enol and keto tautomer of HBT-CN, e) Calculated HOMO and LUMO energy levels of the keto tautomer of the HBT derivatives.

right side of Fig. 3d as an example and that of other HBT derivatives and HBT are shown in Fig. S9. The calculated HOMO/LUMO energy levels are also shown in Fig. 3 eand listed in Table S2. Just like the enol tautomers, for the keto tautomers, the HOMO is mainly located on the phenol ring and the aryl alkynyl moiety, and the LUMO is mainly spread over the phenol ring and the BT ring. Thus, HOMO is more effected by the substituents than the LUMO. For the HBT derivative with large σ, both HOMO and LUMO energy are to be lowered, while the reduction degree of HOMO is larger than that of LUMO, which leads to a increase in the HOMO-LUMO energy gap and thus a blue-shift in the emission spectrum. On the other hand, the HBT derivative with small σ has relatively smaller HOMO-LUMO gap, thus resulting in red-shifted emission. The calculated results confirm the experimentally observed trend that the HBT derivative with smaller σ shows red-shifted fluorescence spectrum and the emission band of the HBT derivative with larger σ hypsochromically shifts.

3.5. Crystal analysis for HBT derivatives

To further elucidate the origin of the difference of photophysical properties of these HBT derivatives, X-ray single-crystal analysis of HBT-H and HBT-Me are performed. The crystallographic data are summarized in Tables S3–S4. In the crystal, the respective three planar π units of HBT-H and HBT-Me (one phenol ring, one BT ring and one aryl alkynyl moiety) are almost in the same plane (Fig. 4). There are the intramolecular H-bonding interactions between the phenolic hydroxyl and the N atom in the BT ring, revealing the stabilization of the enol tautomer in the ground state, which would facilitate to generate the keto tautomer in the excited state. Table 2 shows the

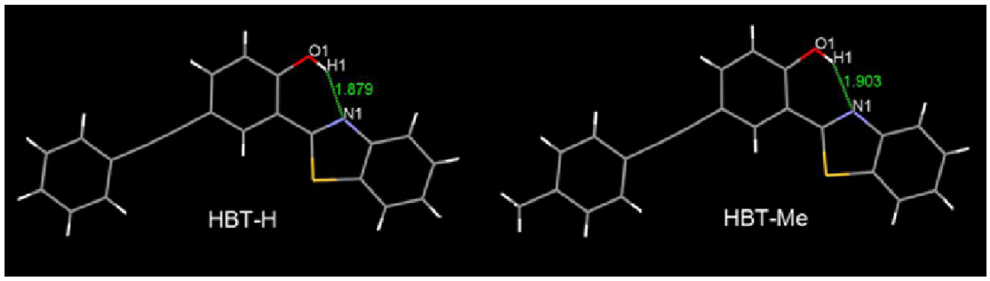

Fig. 4. View of the intramolecular interaction of HBT-Me and HBT-H by Crystal analysis.

Table 2
Hydrogen band parameters for HBT-Me and HBT-H by crystal analysis.

	d (O–H)	d (H···N)	d (N···O)	< O–H···N
HBT-Me	0.820	1.903	2.628	146.96
HBT-H	0.820	1.879	2.608	147.50

H-bond parameters of HBT-H and HBT-Me. The presence of the stronger H-bond reflects the decrease of the O···N distance and of the N···H distance, and the enlarger angle of O–H···N from HBT-Me to HBT-H [23], which is consistent with experimental results and theoretical calculations.

4. Conclusions

A series of HBT derivatives are synthesized by Sonogashira crossing-coupling reaction, and their electronic structures are systematically tuned through various substituents with different σ in the 5-position of the phenol ring. These compounds have a larger π-conjugation framework and show red-shifted absorption/emission vs. HBT. The notable changes in emission spectra of all the derivatives strongly suggest the electronic interaction between the benzothiazole ring and the aryl alkynyl moitey. The HBT derivative with larger σ shows blue-shifted fluorescence spectra with improved fluorescence quantum yield, and the increasing relative intensity ratio of keto emission and enol emission. In protic polar solvent MeOH, the fluorescence difference we observe between HBT-CN, HBT-CF_3 and HBT-CO_2Me might be due to the subtle balance between deprotonation process of phenolic hydroxyl, intermolecular H-bond with solvent molecule and intramolecular H-bond, which cause the anion emission, enol emission and keto emission, respectively. Unlike other HBT derivatives and parent HBT displaying anion emission in PBS medium, HBT-CO_2Me and HBT-CN emit as keto tautomer, which are expected to be applied in various biological aspects. Moreover, the theoretical calculations reproduce the experimentally observed trends. DFT calculations of the enol tautomers show that the HBT derivative with larger σ contains the stronger intramolecular H-bond, which is less likely to be damaged by external factors, and these results are further verified by the crystal analysis. Additionally, DFT calculations of the keto tautomers demonstrate that for the HBT derivative with σ has larger HOMO-LUMO energy gap, which results in blue-shift in the emission spectra.

Acknowledgements

This study was supported by the National Natural Science Foundation of China (21405122), the Natural Science Foundation of Shaanxi (2016JM2009) and the Fundamental Research Funds for the Central Universities (2452015428).

Appendix A. Supplementary data

Supplementary data related to this article can be found at http://dx.doi.org/10.1016/j.dyepig.2016.09.024.

References

[1] Zhao J, Ji S, Chen Y, Guo H, Yang P. Excited state intramolecular proton transfer (ESIPT): from principal photophysics to the development of new chromophores and applications in fluorescent molecular probes and luminescent materials. Phys Chem Chem Phys 2012;14:8803–17.
[2] Mutai T, Tomoda H, Ohkawa T, Yabe Y, Araki K. Switching of polymorph-dependent ESIPT luminescence of an imidazo[1,2-a]pyridine derivative. Angew Chem Int Ed 2008;47:9522–4.
[3] Jiang Y, Wu Q, Chang X. A ratiometric fluorescent probe for hydrogen sulfide imaging in living cells. Talanta 2014;121:122–6.
[4] Murale DP, Kim H, Choi WS, Churchill DG. Highly selective excited state intramolecular proton transfer (ESIPT)-based superoxide probing. Org Lett 2013;15:3946–9.
[5] Kim TI, Kang HJ, Han G, Chung SJ, Kim Y. A highly selective fluorescent ESIPT probe for the dual specificity phosphatase MKP-6. Chem Commun 2009;45:5895–7.
[6] Luo W, Jiang H, Zhang K, Liu W, Tang X, Dou W, et al. A reusable ratiometric two-photon chemodosimeter for Hg^{2+} detection based on ESIPT and its application in bioimaging. J Mater Chem B 2015;3:3459–64.
[7] K-i Sakai, Ishikawa T, Akutagawa T. A blue-white-yellow color-tunable excited state intramolecular proton transfer (ESIPT) fluorophore: sensitivity to polar–nonpolar solvent ratios. J Mater Chem C 2013;1:7866–71.
[8] Park S, Kwon OH, Kim S, Park S, Choi MG, Cha M, et al. Imidazole-based excited-state intramolecular proton-transfer materials: synthesis and amplified spontaneous emission from a large single crystal. J Am Chem Soc 2005;127:10070–4.
[9] Catalán J, Del Valle J, Claramunt R, Sanz D, Dotor J. Photophysics of the 2-(2′-hydroxyphenyl) perimidine: on the fluorescence of the enol form. J Lumin 1996;68:165–70.
[10] Luiz M, Biasutti A, Soltermann AT, Garcia NA. Interaction of UV photostabilizers with singlet molecular oxygen. Polym Degrad Stab 1999;63:447–53.
[11] Sengupta PK, Kasha M. Excited state proton-transfer spectroscopy of 3-hytdroxyflavone and quercetin. Chem Phys Lett 1979;68:382–5.
[12] Liang F, Wang L, Ma D, Jing X, Wang F. Oxadiazole-containing material with intense blue phosphorescence emission for organic light-emitting diodes. Appl Phys Lett 2002;81:4–6.
[13] Barbatti M, Aquino AJ, Lischka H, Schriever C, Lochbrunner S, Riedle E. Ultrafast internal conversion pathway and mechanism in 2-(2'-hydroxyphenyl) benzothiazole: a case study for excited-state intramolecular proton transfer systems. Phys Chem Chem Phys 2009;11:1406–15.
[14] Lochbrunner S, Schultz T, Schmitt M, Shaffer JP, Zgierski MZ, Stolow A. Dynamics of excited-state proton transfer systems via time-resolved photoelectron spectroscopy. J Chem Phy 2001;114:2519.
[15] Abou-Zied OK, Jimenez R, Thompson EH, Millar DP, Romesberg FE. Solvent-dependent photoinduced tautomerization of 2-(2'-hydroxyphenyl) benzoxazole. J Mater Chem A 2002;106:3665–72.
[16] Wu Y, Peng X, Fan J, Gao S, Tian M, Zhao J, et al. Fluorescence sensing of anions based on inhibition of excited-state intramolecular proton transfer. J Org Chem 2007;72:62–70.
[17] Konoshima H, Nagao S, Kiyota I, Amimoto K, Yamamoto N, Sekine M, et al. Excited-state intramolecular proton transfer and charge transfer in 2-(2'-hydroxyphenyl)benzimidazole crystals studied by polymorphs-selected electronic spectroscopy. Phys Chem Chem Phys 2012;14:16448–57.
[18] Das K, Sarkar N, Majumdar D, Bhattacharyya K. Excited-state intramolecular proton transfer and rotamerism of 2-(2′-hydroxyphenyl) benzimidazole. Chem Phys Lett 1992;198:443–8.
[19] Furukawa K, Yamamoto N, Nakabayashi T, Ohta N, Amimoto K, Sekiya H. Changes in the electric dipole moments and molecular polarizabilities of enol and keto forms of 2-(2′-hydroxyphenyl)benzimidazole along the proton transfer reaction path in a PMMA film. Chem Phys Lett 2012;539–540:45–9.
[20] Chen W, Twum EB, Li L, Wright BD, Rinaldi PL, Pang Y. Rotational energy barrier of 2-(2',6'-dihydroxyphenyl)benzoxazole: a case study by NMR. J Org Chem 2012;77:285–90.
[21] Wang H, Zhang H, Abou-Zied O, Yu C, Romesberg F, Glasbeek M. Femtosecond fluorescence upconversion studies of excited-state proton-transfer dynamics in 2-(2′-hydroxyphenyl) benzoxazole (HBO) in liquid solution and DNA. Chem Phys Lett 2003;367:599–608.
[22] Ohshima A, Momotake A, Nagahata R, Arai T. Enhancement of the large stokes-shifted fluorescence emission from the 2-(2'-hydroxyphenyl) benzoxazole core in a dendrimer. J Phys Chem A 2005;109:9731–6.
[23] Mohammed OF, Luber S, Batista VS, Nibbering ET. Ultrafast branching of reaction pathways in 2-(2'-hydroxyphenyl)benzothiazole in polar acetonitrile solution. J Phys Chem A 2011;115:7550–8.
[24] Rini M, Dreyer J, Nibbering ETJ, Elsaesser T. Ultrafast vibrational relaxation processes induced by intramolecular excited state hydrogen transfer. Chem Phys Lett 2003;374:13–9.
[25] Das K, Sarkar N, Ghosh AK, Majumdar D, Nath DN, Bhattacharyya K. Excited-state intramolecular proton transfer in 2-(2-hydroxyphenyl) benzimidazole and-benzoxazole: effect of rotamerism and hydrogen bonding. J Phys Chem 1994;98:9126–32.
[26] Aly SM, Usman A, AlZayer M, Hamdi GA, Alarousu E, Mohammed OF. Solvent-dependent excited-state hydrogen transfer and intersystem crossing in 2-(2'-hydroxyphenyl)-benzothiazole. J Phys Chem B 2015;119:2596–603.
[27] Roberts EL, Dey J, Warner IM. Ground-and excited-state structural orientation of 2-(2'-hydroxyphenyl) benzazoles in cyclodextrins. J Phys Chem 1996;100:19681–6.
[28] Rios M, Rios M. Ab initio study of the hydrogen bond and proton transfer in 2-(2'-hydroxyphenyl) benzothiazole and 2-(2'-hydroxyphenyl) bezimidazole. J Phys Chem A 1998;102:1560–7.
[29] Seo J, Kim S, Park SY. Strong solvatochromic fluorescence from the intramolecular charge-transfer state created by excited-state intramolecular proton transfer. J Am Chem Soc 2004;126:11154–5.
[30] Yang P, Zhao J, Wu W, Yu X, Liu Y. Accessing the long-lived triplet excited

states in bodipy-conjugated 2-(2-hydroxyphenyl) benzothiazole/benzoxazoles and applications as organic triplet photosensitizers for photooxidations. J Org Chem 2012;77:6166–78.
[31] Ma J, Zhao J, Yang P, Huang D, Zhang C, Li Q. New excited state intramolecular proton transfer (ESIPT) dyes based on naphthalimide and observation of long-lived triplet excited states. Chem Commun 2012;48:9720–2.
[32] Yao D, Zhao S, Guo J, Zhang Z, Zhang H, Liu Y, et al. Hydroxyphenyl-benzothiazole based full color organic emitting materials generated by facile molecular modification. J Mater Chem 2011;21:3568–70.
[33] Chen KY, Hsieh CC, Cheng YM, Lai CH, Chou PT. Extensive spectral tuning of the proton transfer emission from 550 to 675 nm via a rational derivatization of 10-hydroxybenzo[h]quinoline. Chem Commun 2006:4395–7.
[34] Cao C, Liu X, Qiao Q, Zhao M, Yin W, Mao D, et al. A twisted-intramolecular-charge-transfer (TICT) based ratiometric fluorescent thermometer with a mega-Stokes shift and a positive temperature coefficient. Chem Commun 2014;50:15811–4.
[35] La Clair JJ. Selective detection of the carbohydrate-bound state of concanvalin A at the single molecule level. J Am Chem Soc 1997;119:7676–84.
[36] Tanpure AA, Srivatsan SG. Synthesis, photophysical properties and incorporation of a highly emissive and environment-sensitive uridine analogue based on the Lucifer chromophore. Chembiochem 2014;15:1309–16.
[37] Ziessel R, Harriman A. Artificial light-harvesting antennae: electronic energy transfer by way of molecular funnels. Chem Commun 2011;47:611–31.
[38] Ulrich G, Ziessel R, Harriman A. The chemistry of fluorescent bodipy dyes: versatility unsurpassed. Angew Chem Int Ed 2008;47:1184–201.
[39] Melhuish WH. Quantum efficiencies of fluorescence of organic substan ces: effect of solvent and concentration of the fluorescent solute. J Phys Chem 1961;65:229–35.
[40] Liu SD, Zhang LW, Liu X. A highly sensitive and selective fluorescent probe for Fe3+ based on 2-(2-hydroxyphenyl)benzothiazole. New J Chem 2013;37:821–6.
[41] Xu Y, Meng J, Meng L, Dong Y, Cheng Y, Zhu C. A highly selective fluorescence-based polymer sensor incorporating an (R,R)-salen moiety for $Zn(^{2+})$ detection. Chem Eur J 2010;16:12898–903.
[42] Ryan ET, Xiang T, Johnston KP, Fox MA. Excited-state proton transfer reactions in subcritical and supercritical water. J Phys Chem 1996;100:9395–402.
[43] Basaric N, Doslic N, Ivkovic J, Wang YH, Veljkovic J, Mlinaric-Majerski K, et al. Excited state intramolecular proton transfer (ESIPT) from phenol to carbon in selected phenylnaphthols and naphthylphenols. J Org Chem 2013;78:1811–23.
[44] Klymchenko AS, Demchenko AP. Multiparametric probing of intermolecular interactions with fluorescent dye exhibiting excited state intramolecular proton transfer. Phys Chem Chem Phys 2003;5:461–8.
[45] Zhang X, Liu J-Y. Solvent dependent photophysical properties and near-infrared solid-state excited state intramolecular proton transfer (ESIPT) fluorescence of 2,4,6-trisbenzothiazolylphenol. Dyes Pigm 2016;125:80–8.
[46] Majumdar P, Zhao J. 2-(2-hydroxyphenyl)-benzothiazole (HBT)-rhodamine dyad: acid-switchable absorption and fluorescence of excited-state intramolecular proton transfer (ESIPT). J Phys Chem B 2015;119:2384–94.
[47] Hansch C, Leo A, Taft R. A survey of Hammett substituent constants and resonance and field parameters. Chem Rev 1991;91:165–95.
[48] Aakeröy CB, Seddon KR. The hydrogen bond and crystal engineering. Chem Soc Rev 1993;22:397–407.
[49] Sakai K, Takahashi S, Kobayashi A, Akutagawa T, Nakamura T, Dosen M, et al. Excited state intramolecular proton transfer (ESIPT) in six-coordinated zinc(ii)-quinoxaline complexes with ligand hydrogen bonds: their fluorescent properties sensitive to axial positions. Dalton Trans 2010;39:1989–95.
[50] Sakai K. Highly efficient solid-state red fluorophores using ESIPT: crystal packing and fluorescence properties of alkoxy-substituted dibenzothiazolylphenols. Crystengcomm 2014;16:3180–5.
[51] Huang Z, Ding S, Yu D, Huang F, Feng G. Aldehyde group assisted thiolysis of dinitrophenyl ether: a new promising approach for efficient hydrogen sulfide probes. Chem Commun 2014;50:9185–7.
[52] Zhao J, Chen J, Liu J, Hoffmann MR. Competitive excited-state single or double proton transfer mechanisms for bis-2, 5-(2-benzoxazolyl)-hydroquinone and its derivatives. Phys Chem Chem Phys 2015;17:11990–9.